HUNGARIAN JOURNAL OF
INDUSTRY AND CHEMISTRY
Vol. 53(2) pp. 107–113 (2025)
hjic.mk.uni-pannon.hu
DOI: 10.33927/hjic-2025-25

HUNGARIAN JOURNAL OF INDUSTRY AND CHEMISTRY
HJIC

THE INFLUENCE OF KEY FDM PRINTING PARAMETERS AND POST-PROCESSING ON THE POROSITY, MICROSTRUCTURE AND MECHANICAL INTEGRITY OF ULTRAFUSE® 17-4 PH STAINLESS STEEL COMPONENTS

GILBERT KIRUI KIPLAGAT[1,2]*

1 Department of Marine Engineering and Maritime Operations, Jomo Kenyatta University of Agriculture and Technology, P.O. Box 62000-00200 Nairobi, KENYA
2 Department of Materials Engineering, University of Pannonia, Egyetem u. 10, Veszprém, 8200, HUNGARY

This study investigates the influence of key printing parameters and post-processing conditions on the printability, microstructure and mechanical integrity of 3D-printed components using an Ultrafuse ® 17-4 PH stainless steel filament and metal Fused Deposition Modeling (FDM). A full-factorial-type of experimental design was implemented, varying layer height, print structure and infill orientation. Specimens were designed based on ASTM D368 type V. Green parts were printed using a Rat Rig V-Core 3 FDM 3D printer as well as evaluated via computed tomography (CT) to analyze and characterize the porosity in the 3D printed parts. The results showed that 'Only-infill' printed structures and layer heights of ≤25% of the nozzle diameter led to a significant decrease in average porosity levels with values recorded below 3.8 % (V/V). 'All-wall' specimens exhibited a comparatively higher level of porosity attributed to an increased cooling rate-to-deposition time ratio that weakened interlayer bonding and promoted void alignment along bonding lines. Uneven shrinkage, surface bulging and geometric irregularities were evident across the printed samples, primarily resulting from non-uniform binder distribution and inhomogeneous temperature gradients during fabrication. The experimental findings established a strong correlation between printing parameters, microstructural evolution and part densification. These results provide a technical framework for optimizing process parameters to achieve high-density, low-porosity stainless steel components fabricated through metal FDM, thereby enhancing the reliability and performance of additively manufactured metallic parts.

Keywords: FDM, sintering, debinding, porosity, CT analysis, microstructure, Ultrafuse ® 17-4 PH

1. Introduction

A wide range of conventional technologies have been applied to manufacture metallic components across different industrial segments, including forming processes, subtractive manufacturing technologies, material cutting and shaping operations which have specific features as well as characteristics in the production of various end-user products. With their excellent capabilities in manufacturing, characteristic drawbacks arising from their technological limitations do exist. These limitations, for instance, include material waste, high production cost, their time-consuming nature and inability to produce complex structures. Since these drawbacks need to be resolved, researchers are continuously developing and improving technologies to address some of them, one of these technologies is Additive Manufacturing (AM).

In contrast to conventional methods, AM uses a different approach to building products. It builds the products bottom-up by joining/fusing and binding materials layer by layer. This technology has an immense ability to produce complex products, for instance, a new suppressor used by the US Army can only be manufactured by Metal Additive Manufacturing. A wide range of materials including thermoplastics, composites, ceramics and metals can be used in this technology based on machine characteristics.

Recent advancements in computer-aided technologies such as CAD, CAM and CAE have revolutionized product development enabling the efficient handling of complex geometries and virtual design models [1]-[4]. With the help of such software, it is now possible to generate photo-realistic images and render models according to elaborate shading algorithms [5],[6]. These techniques form an integral part in AM processes [7] and the design-to-production pipeline, laying a good foundation for AM, a process that relies on

Received: 28 June 2025; Revised: 30 Oct 2025;
Accepted: 3 Nov 2025
*Correspondence: kiruigilbert57@gmail.com

digital models to fabricate a physical object through the successive deposition of materials [6,8,9].

AM technologies can be divided into three broad categories referred to as resin-based, extrusion-based and powder-based [10]. Resin-based methods, including Material Jetting and Vat Photopolymerization, use photosensitive materials that undergo polymerization when exposed to UV radiation [11]. Extrusion-based techniques, i.e. Fused Deposition Modeling (FDM) and Directed Energy Deposition (DED), rely on heated filaments or granules deposited layer by layer [12],[13]. Powder-based processes, like Powder Bed Fusion (PBF) and Binder Jetting, use thermal or chemical sources to bind or sinter powder layers [14].

Although the availability of printable materials remains a limitation in AM, much progress with polymers (PLA, ABS, PVA, PA, PET, PETG), ceramics and advanced metal-filled filaments among other currently limited materials has been made over recent years [15],[16]. The mechanical properties of printed parts are highly dependent on printing parameters and post-printing processes. The layer height, infill density, print structure and raster angle are key parameters [17]-[20]. Several studies have demonstrated that fine-tuning these printing parameters can significantly improve the mechanical performance of printed parts [21]-[25].

More recently, studies have demonstrated that metal-based filaments such as 17-4PH SS with optimized pre- and post-processing parameters can be used to achieve high-strength components using Metal FDM (MFDM). Improved debinding and sintering significantly enhance tensile strength and minimize average porosities [26]. The infill pattern, print speed and print orientation affect the mechanical properties of printed parts [27].

With these findings, the effects of parameter interdependencies make it difficult to isolate individual effects [28]. Abe et al. [29] concluded that sintered MFDM parts could potentially meet industrial standards. To achieve this, further research is necessary to minimize anisotropic shrinkage and improve structural integrity.

To overcome these shortcomings, future studies should focus on the optimization of both printing parameters and post-printing processes. Similarly, an in-depth investigation into layer adhesion and anisotropic shrinkage with the aim of developing innovative approaches to enhance the mechanical properties of printed components is highly recommended [13],[18].

FDM has emerged as a disruptive technology in engineering, capable of producing complex geometries with reduced material waste [30]. However, limitations persist in achieving structural density and mechanical integrity in metal-based FDM components. This research addresses these challenges through the systematic optimization of printing and thermal post-processing parameters.

2. Experimental

2.1. Materials and methods

Full factorization, one type of experimental design, which considers every possible combination of parameters and levels, is preferred for this study. Three parameters are considered in this study, namely infill pattern (0 and 45°), layer height (25, 50 and 75% of the nozzle diameter) and print structure ('All-wall' (AW) and 'Only-infill' (OI)). A nozzle diameter of 0.4 mm was used. To ensure reliable data, three specimens from each set were printed.

A Rat Rig V-Core 3 FDM 3D printer was used to print all the specimens designed using CAD (Fusion), in accordance with the ASTM D368 type V standard. Expected dimensional shrinkage was factored in during their design as guided by the filament supplier. A commercially available Ultrafuse® 17-4 PH 1.75 ± 0.050 mm stainless-steel filament supplied by BASF 3D Printing Solutions GmbH was utilized as the feedstock.

The 3D model was processed using a PrusaSlicer slicing algorithm in a G-code format, which defined the optimal print head paths for each layer. Printer setup included bed homing, build-plate mounting and the use of a thin layer of adhesive (hair spray) to minimize part warping and improve adhesion. Following a trial and error approach, 240 °C nozzle and 110 °C build-plate temperatures were found to be ideal for printing metal-based filaments. A slower speed, as guided by the filament supplier, was chosen to enhance precision and interlayer bonding. Close attention was paid to the prints during printing to avoid nozzle clogging and part warping. Brittle green parts were allowed to cool for a minute on the build plate before being carefully detached and maintained under ambient conditions.

2.2. Computed tomography (CT): porosity analysis

The sample volume required for the aforementioned analysis was examined with the XT H 225 ST computed tomography system produced by Nikon. An accelerating voltage of 165 kV was applied which is ideal for high-resolution CT imaging. Different CT images were extracted for object reconstruction. 3D objects reconstructed from obtained CT images are presented in *Figures 1-5* using VG Studio Max 2024/1 CT-Pro porosity analysis software.

3. Results and analysis

The study analyzed how three key 3D printing parameters, namely layer height, infill orientation and structure type, affect the porosity of green parts and the mechanical behavior of sintered parts.

Note: Box and whisker plots were used to visualize the porosity analysis across the tested parameters

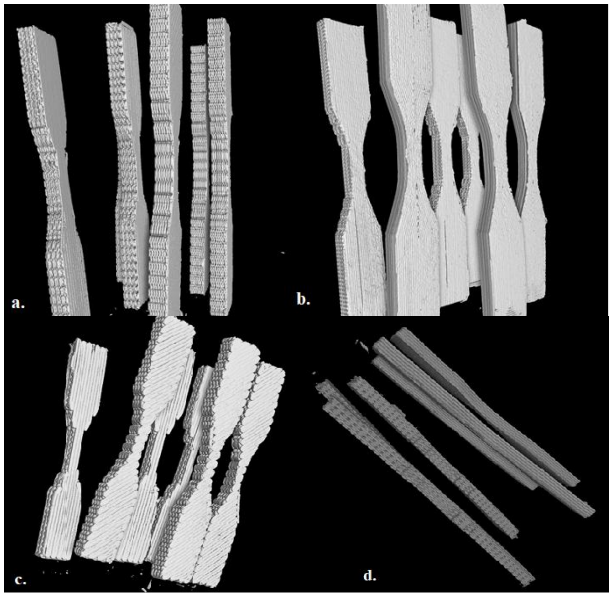

Figure 1: Reconstructed 3D images of different specimens following CT scans

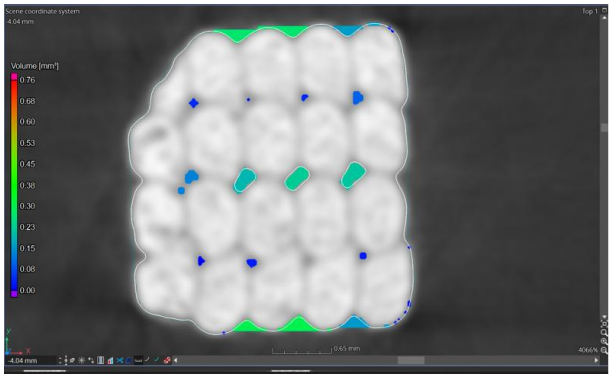

Figure 2: 2D top cross-section of a 75-0-AW specimen

(*Figure 6-11*). A box and whisker plot shows the distribution of the porosity percentage (V/V) for the tested parameters. Each box plot represents the middle 50% of the data, that is, the lower (Q1) to the upper quartile (Q3). The lines inside the boxes indicate the medians. The whiskers illustrate the minimum and maximum values of the data but exclude the outliers, namely strange data values which are far lower or higher when compared to the rest of the data points, and "X"s indicate the means.

It was observed that decreasing layer height significantly decreased porosity, with the effect dependent on the infill structure *(Figure 6)*. The 'All-wall' configuration consistently exhibited lower porosity than the 'Only-infill' structure for comparable processing parameters.

The print structure significantly influences the porosity. Specimens with 'All-wall' structures exhibited a slightly lower average porosity percentage compared to their 'Only-infill' counterparts regardless of the layer

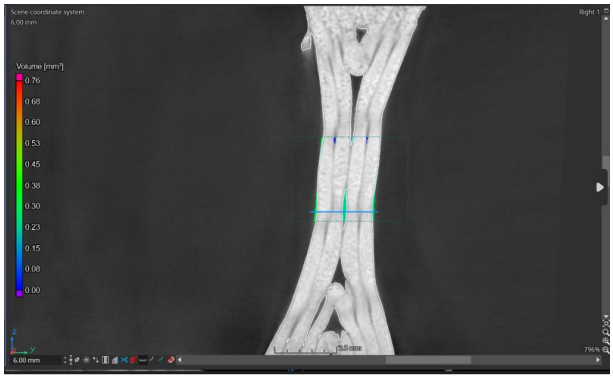

Figure 3: 2D longitudinal section of a 75-0-AW specimen

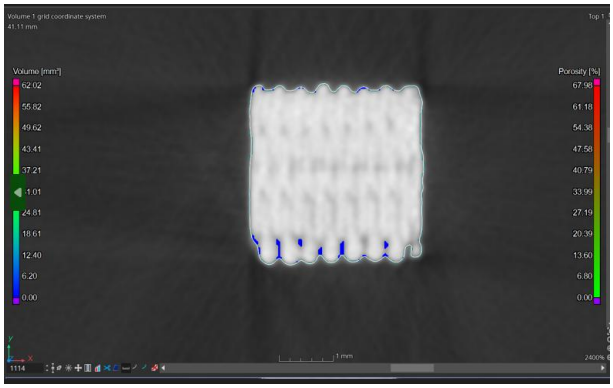

Figure 4: 2D top cross-section of a 25-45-OI specimen

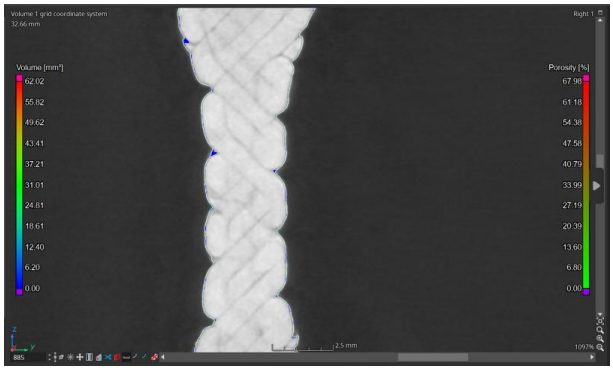

Figure 5: 2D longitudinal section of a 25-45-OI specimen

height or infill orientation as shown in *Figure 7*, but the porosity percentages were widely distributed. The influence of infill orientation (0 and 45°) was relatively weak in comparison, though the porosity percentage of the 45° pattern was slightly lower (*Figure 8*).

The results showed that a decrease in the layer height significantly decreases porosity. The lowest porosity values were observed when the layer height was 25% of the nozzle diameter. As the layer height increased, the porosity consistently increased, reaching values as high as 3.8% for the 75-0-AW specimen. These findings are illustrated in *Figures 9-11*.

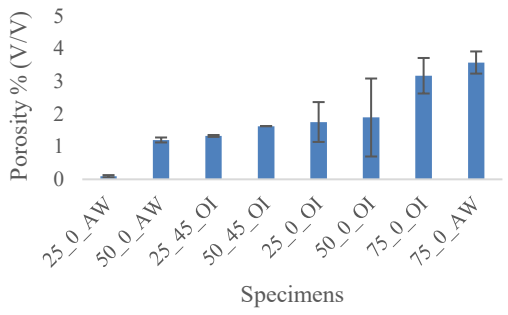

Figure 6: Average porosity values for parallel specimens with comparable parameter configurations

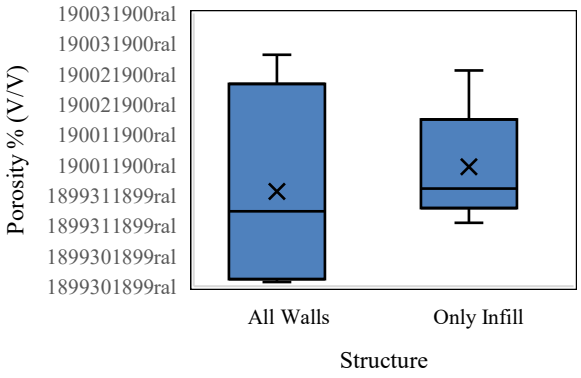

Figure 7: Relationship between structure and porosity % (V/V)

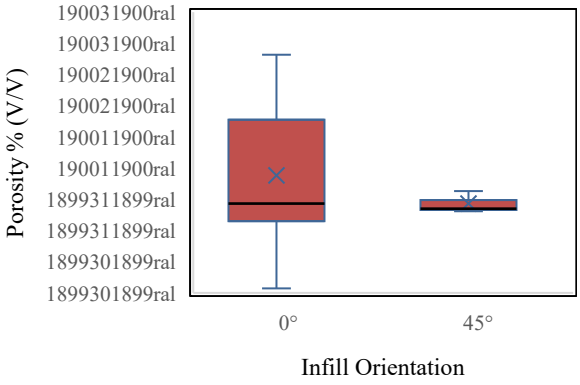

Figure 8: Relationship between infill orientation and porosity % (V/V)

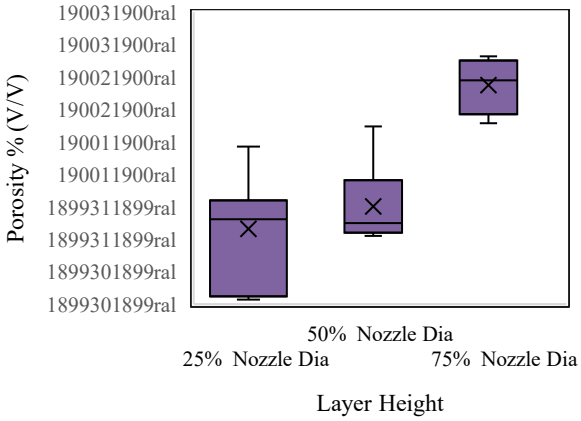

Figure 9: Relationship between layer height and porosity % (V/V)

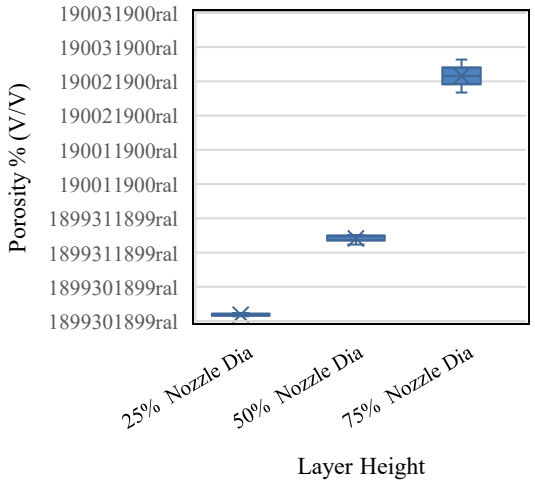

Figure 10: Relationship between Layer height and Porosity % (V/V) for the 'All-walled' structures

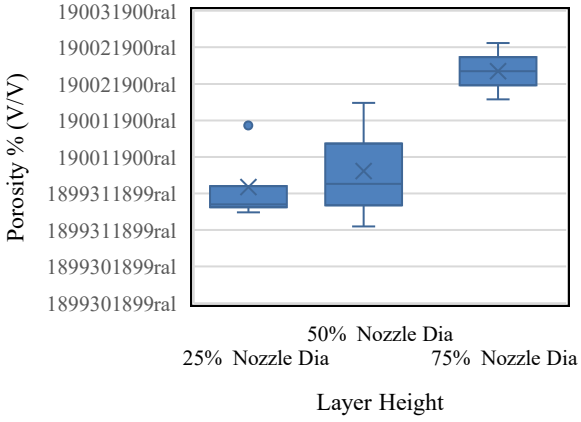

Figure 11: Relationship between layer height and porosity % (V/V) for the 'Only-infill' structures

4. Discussion

Uneven shrinkage, surface bulging and irregularities were observed. This inconsistent surface morphology with asymmetric dimensional changes, part warping and layer delamination can be attributed to non-uniform binder distribution during filament fabrication as well as inhomogeneous temperature profiles during part printing.

Furthermore, void distribution in all the tested green parts was observed to be homogeneously aligned along the fusion lines. However, the void sizes varied significantly across the examined parts, illustrating how important it is to optimize the printing parameters.

The presence of these voids not only compromises mechanical performance but also influences the subsequent sintering behavior of the printed components. Smaller, evenly distributed voids can be healed effectively during sintering, whereas larger, irregular voids may persist as pores, leading to reduced density and anisotropic shrinkage. Therefore, understanding the origin and evolution of such voids during the green state is vital to achieve high-quality final parts.

The high porosity in 'All-wall' specimens is attributed to an increased ratio of the cooling rate to deposition time. In such parameter configurations, the nozzle traverses a slightly longer distance during the deposition of a single layer, thereby increasing the printing time per layer. The increased time interval between depositing successive layers results in a larger temperature gradient which weakens interlayer bonding. This phenomenon is particularly evident in the regions between adjacent walls.

The directional cooling patterns in 'All-wall' specimens tend to generate localized stress accumulation along the wall interfaces which may further promote the formation of microvoids. The interaction between these thermal and mechanical effects reinforces the concept that print path and wall configuration strongly influence the bonding efficiency as well as density uniformity within the printed structure.

On the other hand, the alternating nature of the infill deposition in 'Only-infill' patterns allows material flow into the void lines of the previous deposited layer, thus a lower porosity percentage is observed. The lower porosity percentage can also be attributed to the improved thermal bonding conditions due to the shorter travel distance of the print head and smaller thermal differences during cooling intervals.

This deposition strategy enhances material continuity and ensures that each successive layer benefits from a more uniform thermal history. Consequently, superior layer adhesion is exhibited and the likelihood of interfacial separation reduced in the print. Such process stability is critical when high-density parts with reliable mechanical performance are sought.

5. Conclusions

The results provide valuable insights into the complex relationship between the parameters and quality of the 3D printed parts.

Porosity analysis showed that voids were largely aligned along fusion lines but the void size varied significantly depending on the print configurations. 'All-wall' green parts exhibited a higher average porosity percentage compared to their 'Only-infill' counterparts. This lower porosity percentage was linked to a higher cooling rate-to-deposition time ratio which led to poor thermal bonding and reduced interlayer fusion. In contrast, specimens with a lower layer height, especially 25% of the nozzle diameter, exhibited the lowest porosity levels due to enhanced heat retention and improved interlayer fusion. Significantly, the recorded porosities were lower than 3.8 % (V/V) for all specimens.

These findings collectively emphasize the intricate interplay between material flow, temperature control and the deposition sequence. It is evident that even minor alterations to the layer height or infill pattern can strongly influence the final density and dimensional accuracy of the part. The correlation between process parameters and porosity highlights the necessity of precise calibration before large-scale manufacturing.

A combination of parameters for 'Only-infill' structures, infill orientation of 0° and a low layer height may well enhance densification, thus would be ideal for low-porosity printing and high-density applications.

Moreover, these optimized conditions may also contribute to improved mechanical isotropy, the reduced accumulation of residual stress and more predictable sintering shrinkage. Future research can expand on this by exploring hybrid parameter configurations that combine wall-infill interactions with controlled cooling systems to achieve even finer microstructural control.

This study outlined the effects of varying the printing parameter configurations and sintering conditions in terms of part densification and mechanical reliability. Beyond the laboratory scale, the implications of these results extend to industrial additive manufacturing, where achieving near-full density is essential for load-bearing or functional metallic components.

A systematic approach integrating parameter tuning, real-time thermal monitoring and post-process analysis would therefore pave the way toward producing high-performance printed metals with minimal defects suitable for structural applications.

Acknowledgement

The research was supported by Dr. Attila Egedy & András Kámán from the Department of Materials Engineering at the University of Pannonia in Veszprém, Hungary.

REFERENCES

[1] Groover, M.P.: Automation, Production systems, and computer-intergrated manufacturing, India (Pearson Education), 2016

[2] Liou, F.W.: Rapid prototyping and engineering applications: A toolbox for prototype development (CRC Press, Boca Raton, FL, USA), 2008, ISBN: 9780849334092

[3] Magrab, E.B.; Gupta, S.K.; McCluskey, F.P.; Sandborn, P.: Integrated product and process design and development (CRC Press, Boca Raton, FL, USA), 2010, ISBN: 9781420070606

[4] Gibson, I.: Rapid prototyping: from product development to medicine and beyond, *Virtual Phys. Prototyp.*, 2006, **1**(1), 31–42, DOI: 10.1080/17452750500271298

[5] Kurowski, P.M.: Finite element analysis for design engineers (3rd edition) (SAE International, Warrendale, PA, USA), 2022, ISBN: 9781468605358

[6] Shahrubudin, N.; Lee, T.C.; Ramlan, R.: An overview on 3D printing technology: Technological, materials, and applications, *Procedia Manuf.*, 2019, **35**, 1286–1296, DOI: 10.1016/j.promfg.2019.06.089

[7] Kruth, J.-P.; Leu, M.C.; Nakagawa, T.: Progress in additive manufacturing and rapid prototyping, *CIRP Ann. Manuf. Technol.*, 1998, **47**(2), 525–540, DOI: 10.1016/S0007-8506(07)63240-5

[8] ISO/ASTM 52900:2021: Additive manufacturing - General principles - Fundamentals and vocabulary

[9] Gibson, I., Rosen, D.; Stucker, B.: Additive manufacturing technologies: 3D printing, rapid prototyping, and direct digital manufacturing (2nd edition) (Springer, New York, NY, USA), 2015, DOI: 10.1007/978-1-4939-2113-3

[10] ASTM F2792-10 (2010): Standard terminology for additive manufacturing technologies, ASTM International

[11] Bikas, H.; Stavropoulos, P.; Chryssolouris, G.: Additive manufacturing methods and modelling approaches: A critical review, *Int. J. Adv. Manuf. Technol.*, 2016, **83**(1-4), 389–405, DOI: 10.1007/s00170-015-7576-2

[12] Lipson, H.; Kurman, M.: Fabricated: The new world of 3D printing (Wiley, Hoboken, NJ, USA), 2013, ISBN: 9781118350638

[13] Panda, S.K.; Rath, K.C.; Mishra, S.; Khang, A.: Revolutionizing product development: The growing importance of 3D printing technology, *Mater. Today Proc.*, 2023, DOI: 10.1016/j.matpr.2023.10.138

[14] Gebhardt, A.; Hötter, J.-S.: Additive Manufacturing: 3D printing for prototyping and manufacturing (Hanser Publications, Munich, Germany), 2016, ISBN: 9781569905821

[15] Ngo, T.D.; Kashani, A.; Imbalzano, G.; Nguyen, K.T.Q.; Hui, D.: Additive manufacturing (3D printing): A review of materials, methods, applications and challenges, *Compos. B. Eng.*, 2018, **143**, 172–196, DOI: 10.1016/j.compositesb.2018.02.012

[16] Gonzalez-Gutierrez, J.; Cano, S.; Schuschnigg, S.; Kukla, C.; Sapkota, J.; Holzer, C.: Additive manufacturing of metallic and ceramic components by the material extrusion of highly-filled polymers: A review and future perspectives, *Materials*, 2018, **11**(5), 840, DOI: 10.3390/ma11050840

[17] Dezaki, M.L.; Serjouei, A.; Zolfagharian, A.; Fotouhi, M.; Moradi, M.; Ariffin, M.K.A.; Bodaghi, M.: A review on additive/subtractive hybrid manufacturing of directed energy deposition (DED) process, *Adv. Powder Mater.*, 2022, **1**(4), 100054, DOI: 10.1016/j.apmate.2022.100054

[18] Park, S.; Shou, W.; Makatura, L.; Matusik, W.; Fu, K.K.: 3D printing of polymer composites: Materials, processes, and applications, *Matter*, 2022, **5**(1), 43–76, DOI: 10.1016/j.matt.2021.10.018

[19] Singh, A.K.; Chauhan, S.: Technique to enhance FDM 3D metal printing, *Bonfring Int. J. Ind. Eng. Manag. Sci.*, 2016, **6**(4), 128–134, DOI: 10.9756/BIJIEMS.7574

[20] Hsueh, M.-H.; Lai, C.-J.; Chung, C.-F.; Wang, S.-H.; Huang, W.-C.; Pan, C.-Y.; Zeng, Y.-S.; Hsieh, C.-H.: Effect of printing parameters on the tensile properties of 3D-printed polylactic acid (PLA) based on fused deposition modeling, *Polymers*, 2021, **13**(14), 2387, DOI: 10.3390/polym13142387

[21] Basak, A.; Lee, A.; Pramanik, A.; Neubauer, K.; Prakash, C.; Shankar, S.: Material extrusion additive manufacturing of 17–4 PH stainless steel: effect of process parameters on mechanical properties, *Rapid Prototyp. J.*, 2023, **29**(5), 1097–1106, DOI: 10.1108/RPJ-05-2022-0169

[22] Anand Kumar, S.; Shivraj Narayan, Y.: Tensile testing and evaluation of 3D-printed PLA specimens as per ASTM D638 type IV standard, in Innovative Design, Analysis and Development Practices in Aerospace and Automotive Engineering (I-DAD 2018), Chandrasekhar, U.; Yang, L.-J.; Gowthaman, S. (Eds) (Springer Singapore, Singapore), 2019, pp. 79–95, DOI: 10.1007/978-981-13-2718-6_9

[23] Appalsamy, T.; Hamilton, S.L.; Kgaphola, M.J.: Tensile test analysis of 3D printed specimens with varying print orientation and infill density, *J. Compos. Sci.*, 2024, **8**(4), 121, DOI: 10.3390/jcs8040121

[24] Zisopol, D.G.; Nae, I.; Portoaca, A.I.; Ramadan, I.: A theoretical and experimental research on the influence of FDM parameters on tensile strength and hardness of parts made of polylactic acid, *Eng. Technol. Appl. Sci. Res.*, 2021, **11**(4), 7458–7463, DOI: 10.48084/etasr.4311

[25] Seensattayawong, P.; Suwanpreecha, C.; Boonlert, N.; Songkuea, S.; Manonukul, A.: The effect of printing parameters on the properties of 17-4 PH stainless steel fabricated by material extrusion additive manufacturing, *J. Met. Mater. Miner.*, 2024, **34**(2), 1804, DOI: 10.55713/jmmm.v34i2.1804

[26] Gonzalez-Gutierrez, J.; Arbeiter, F.; Schlauf, T.; Kukla, C.; Holzer, C.: Tensile properties of sintered 17-4PH stainless steel fabricated by material extrusion additive manufacturing, *Mater. Lett.*, 2019, **248**, 165–168, DOI: 10.1016/j.matlet.2019.04.024

[27] Auffray, L.; Gouge, P.-A.; Hattali, L.: Design of experiment analysis on tensile properties of PLA samples produced by fused filament fabrication, *Int. J. Adv. Manuf. Technol.*, 2022, **118**(11-12), 4123–4137, DOI: 10.1007/s00170-021-08216-7

[28] DebRoy, T.; Wei, H.L.; Zuback, J.S.; Mukherjee, T.; Elmer, J.W.; Milewski, J.O.; Beese, A.M.; Wilson-Heid, A.; De, A.; Zhang, W.: Additive manufacturing of metallic components – Process, structure and properties, *Prog. Mater. Sci.*, 2018, **92**, 112–224, DOI: 10.1016/j.pmatsci.2017.10.001

[29] Abe, Y.; Kurose, T.; Santos, M.V.A.; Kanaya, Y.; Ishigami, A.; Tanaka, S.; Ito, H.: Effect of layer directions on internal structures and tensile properties of 17-4PH stainless steel parts fabricated by fused deposition of metals, *Materials*, 2021, **14**(2), 243, DOI: 10.3390/ma14020243

[30] Roshchupkin, S.; Kolesov, A.; Tarakhovskiy, A.; Tishchenko, I.: A brief review of main ideas of metal fused filament fabrication, *Mater. Today Proc.*, 2021, **38**(4), 2063–2067, DOI: 10.1016/j.matpr.2020.10.142